

## Distances between the b-subunits in the tether domain of F<sub>0</sub>F<sub>1</sub>-ATP synthase from *E. coli*

Stefan Steigmiller<sup>a</sup>, Michael Börsch<sup>b</sup>, Peter Gräber<sup>a</sup>, Martina Huber<sup>c,\*</sup>

<sup>a</sup>Institut für Physikalische Chemie, Universität Freiburg, Germany

<sup>b</sup>3. Physikalisches Institut, Universität Stuttgart, Germany

<sup>c</sup>Department of Molecular Physics, Leiden University, P.O. Box 9504, 2300 RA Leiden, The Netherlands

Received 7 October 2004; received in revised form 15 March 2005; accepted 16 March 2005

Available online 20 April 2005

### Abstract

The arrangement of the b-subunits in the holo-enzyme F<sub>0</sub>F<sub>1</sub>-ATP synthase from *E. coli* is investigated by site-directed mutagenesis spin-label EPR. F<sub>0</sub>F<sub>1</sub>-ATP synthases couple proton translocation with the synthesis of ATP from ADP and phosphate. The hydrophilic F<sub>1</sub>-part and the hydrophobic membrane-integrated F<sub>0</sub>-part are connected by a central and a peripheral stalk. The peripheral stalk consists of two b-subunits. Cysteine mutations are introduced in the tether domain of the b-subunit at b-40, b-51, b-53, b-62 or b-64 and labeled with a nitroxide spin label. Conventional (9 GHz), high-field (95 GHz) and pulsed EPR spectroscopy reveal: All residues are in a relatively polar environment, with mobilities consistent with helix sites. The distance between the spin labels at each b-subunit is 2.9 nm in each mutant, revealing a parallel arrangement of the two helices. They can be in-register but separated by a large distance (1.9 nm), or at close contact and displaced along the helix axes by maximally 2.7 nm, which excludes an in-register coiled-coil model suggested previously for the b-subunit. Binding of the non-hydrolysable nucleotide AMPPNP to the spin-labeled enzyme had no significant influence on the distances compared to that in the absence of nucleotides.

© 2005 Elsevier B.V. All rights reserved.

**Keywords:** H<sup>+</sup>-ATP synthase; b-subunit; Site-directed spin labeling; MTSL; EPR spectroscopy; DEER

### 1. Introduction

F<sub>0</sub>F<sub>1</sub>-ATP synthases catalyze the proton transport-coupled synthesis of ATP from ADP and phosphate in bacteria, chloroplasts and mitochondria [1]. The enzyme consists of two large domains: a membrane-integrated F<sub>0</sub>-part catalyzing the transmembrane proton transport and a hydrophilic F<sub>1</sub>-part containing the nucleotide and phosphate binding sites. In the F<sub>0</sub>F<sub>1</sub>-ATP synthase from *E. coli*, the F<sub>1</sub>-part has a subunit composition of  $\alpha_3\beta_3\gamma\delta\epsilon$  (see Fig. 1a). The

F<sub>0</sub>-part consists of  $ab_2c_{10-14}$  [2] and the c-subunits form a ring in the membrane [3].

According to the ‘binding change’ theory, the three catalytic nucleotide binding sites of the  $\beta$ -subunits undergo conformational changes, adopting in subsequent steps the ‘open’, ‘tight’ and ‘loose’ conformation. This is accomplished by sequential “docking–undocking” steps of the  $\gamma$ -subunit to the three different  $\alpha\beta$ -pairs, i.e. by a rotation of the  $\gamma$ -subunit which synchronizes the catalytic reaction at the three catalytic sites [4]. The high resolution X-ray structure supported this mechanism [5] and rotation of the  $\gamma$ -subunit during ATP hydrolysis was demonstrated [6,7] and visualized by video-microscopy [8].

With respect to proton transport-coupled ATP synthesis in the holo-enzyme, it was suggested that the  $\gamma$ -subunit is connected with the ring of c-subunits and that proton transport through the enzyme is accomplished by rotation of the c-ring in the membrane. As the c-ring

*Abbreviations:* AMPPNP, adenosine-5-( $\beta,\gamma$ -imido) triphosphate; DEER, double electron–electron resonance; EPR, electron paramagnetic resonance; MTSL, (1-oxyl-2,2,5,5-tetramethyl- $\Delta$ 3-pyrroline-3-methyl) methanethiosulfonate; TMR-M, tetramethylrhodamine-5-maleimide

\* Corresponding author. Tel.: +31 71 527 5560; fax: +31 71 527 5819.

E-mail address: [mhuber@molphys.leidenuniv.nl](mailto:mhuber@molphys.leidenuniv.nl) (M. Huber).

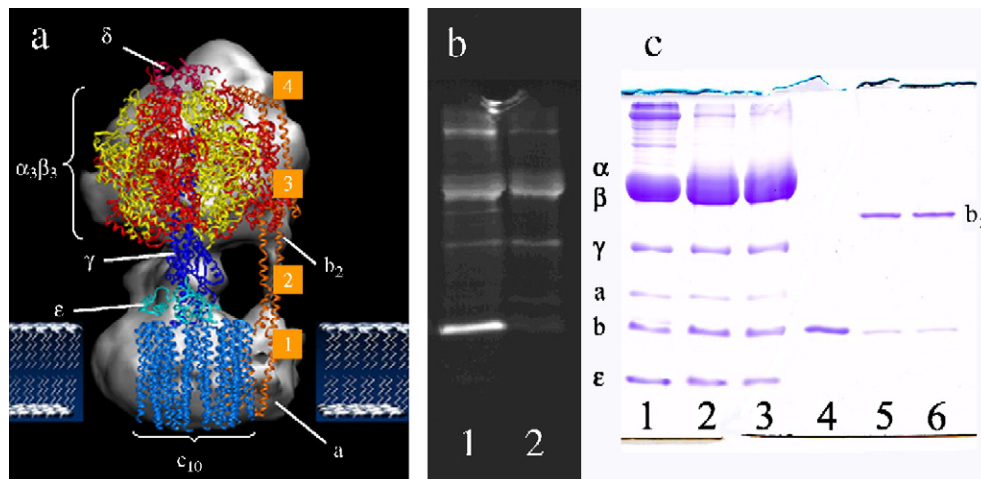


Fig. 1. (a) Membrane-embedded F<sub>0</sub>F<sub>1</sub>-ATP synthase from *E. coli* derived from homology modeling [17] and electron microscopy [18]. According to [23], the b-subunit (orange) can be divided into the transmembrane domain (pictured as <1>), tether domain <2>, dimerization domain <3> and δ-binding domain <4>. Each b-subunit was labeled with the nitroxide spin-label MTSL at residues 40, 51, 53, 62 and 64 which are located in the tether or dimerization domain, respectively. (b) Fluorograms of electrophoretic separation (SDS-PAGE) of the subunits of F<sub>0</sub>F<sub>1</sub>-ATP synthase. Lane 1: F<sub>0</sub>F<sub>1</sub> labeled with TMR-M. Mainly, the b-subunits are labeled. Subunits α, β and γ show weak fluorescence intensities. Other subunits are not labeled. Lane 2: Spin-labeled F<sub>0</sub>F<sub>1</sub> was labeled with TMR-M. Subunit b shows very weak fluorescence intensity; the intensities of other subunits are comparable to lane 1. (c) SDS-PAGE of cross-linking experiment. Lane 1: F<sub>0</sub>F<sub>1</sub> without cross-linking treatment. Subunit c ran out of the gel; the δ-subunit can be seen as a weak band above the b-subunit. Lanes 2 and 3: F<sub>0</sub>F<sub>1</sub> treated with 50 μM CuCl<sub>2</sub>. The reaction was stopped by the addition of 2 mM EDTA after 30 min and 120 min, respectively. No b-dimer can be seen. Lane 4: truncated b-subunit b<sub>34-156</sub>T62C (without residues 1 to 33). Lane 5 and 6: b<sub>34-156</sub>T62C treated with 50 μM CuCl<sub>2</sub>. The reaction was stopped by adding 2 mM EDTA after 30 min and 120 min, respectively, indicating cross-linking (>90% of b-dimer).

interacts with the γ- and ε-subunits, this drives the rotation of the γ-subunit in the F<sub>1</sub>-part. Correspondingly, the γεc<sub>10-14</sub> complex is called “rotor”, α<sub>3</sub>β<sub>3</sub>δab<sub>2</sub> the “stator” [9–12].

Quantitative models describing the generation of the required power for ATP synthesis have been presented [13–15]. Recently, it has been shown with single molecule spectroscopy that during proton transport-driven ATP synthesis, the γ-subunit rotates relative to the stator subunits and that the direction of rotation is reversed during ATP hydrolysis [16,17] (a model of F<sub>0</sub>F<sub>1</sub>-ATP synthase is shown in Fig. 1a combining data from electron microscopy [18] and a homology model [17]).

The movement of the rotor part in the enzyme requires a firm connection between the stator subunits. According to the current structural models, the two b-subunits connect the membrane-integrated stator part (a-subunit) with the hydrophilic stator part (α<sub>3</sub>β<sub>3</sub>δ-subunits). Electron microscopy showed that F<sub>1</sub> and F<sub>0</sub> are linked by a central (γ- and ε-subunit) and a peripheral (b-subunits) second stalk [18–20]. A high-resolution X-ray structure of the b-subunits in the holo-enzyme is not available yet, however some data were published on the structure of parts of the subunit and its interaction with the F<sub>1</sub>-part [21,22]. The b-subunit can be divided into 4 major parts: the N-terminal transmembrane domain (see domain <1> in Fig. 1a, residues 1 to 22), followed by the tether domain (<2>, residues 23 to 52), the dimerization domain (<3>, residues 53 to 122) [23] and the δ-binding domain (<4>, residues 123 to 156) [24]. The structure of an isolated fragment of the b-subunit comprising residues 1 to 34 has been solved

by NMR, revealing a hydrophobic membrane-spanning α-helix [21]. Recently, the binding strength of the b-subunits to the F<sub>1</sub>-part was determined [25,26]. Further biochemical approaches such as circular dichroism spectroscopy, chemical cross-linking, analytical ultracentrifugation and deletion analysis revealed that the structure of the peripheral stalk consists of a highly extended conformation containing ~80% α-helix [27–34].

Structural information about the b-subunit in the holo-enzyme is needed to understand the role of the b-subunit in the stator part of the enzyme. The tether domain was used for fluorescence labeling in a recent single-molecule investigation of proton transport-coupled ATP synthesis [17], however very little is known about its structure.

We used a site-directed mutagenesis spin labeling EPR approach to investigate the structure of the b-subunits in the holo-enzyme. Previous spin-label EPR studies have targeted the β-subunit in F<sub>1</sub>-ATPase using native cysteines [35] and mutagenesis to introduce spin labels in the isolated soluble b-subunit of ATPase [36,37].

In the present work, a series of mutants along a stretch extending from the tether domain to the dimerization domain of the b-subunit was prepared. As there are two b-subunits in the enzyme, mutagenesis to replace one codon of the b-gene by the cysteine-codon results in the substitution of two cysteines in the holo-enzyme. The mutants prepared were b-I40C, b-H51C, b-D53C, b-T62C and b-Q64C. In each case, the holo-enzyme was spin labeled with the nitroxide label MTSL, resulting in the spin-labeled mutants F<sub>0</sub>F<sub>1</sub>-bI40C, F<sub>0</sub>F<sub>1</sub>-bH51C, F<sub>0</sub>F<sub>1</sub>-bD53C, F<sub>0</sub>F<sub>1</sub>-bT62C and F<sub>0</sub>F<sub>1</sub>-bQ64C.

Advanced EPR techniques were used to obtain structural parameters of the b-subunit. For all mutants, liquid solution X-band (9 GHz) EPR, frozen solution X- and W-band (95 GHz) EPR, and a pulsed X-band double electron–electron resonance (DEER) [38] EPR technique were used to determine the properties of the spin labels and the distances between paramagnetic centers. DEER is a recent method in EPR to determine distances in the nanometer range, which has been demonstrated to yield reliable distance information on doubly spin-labeled chemical systems [38] and proteins of known structure [39,40].

## 2. Materials and methods

### 2.1. Enzyme preparation

F<sub>0</sub>F<sub>1</sub>-ATP synthases from *E. coli* carrying one of the cysteine mutations b-I40C, b-H51C, b-D53C, b-T62C and b-Q64C, respectively, were prepared separately according to [16] using the plasmid pRR76 expressed in the strain RA1 and stored in liquid nitrogen.

### 2.2. Site-directed spin labeling

The two cysteines of the b-subunits were labeled with the spin-label MTSL (Toronto Research Chemicals, Toronto, Canada). MTSL was dissolved in dimethyl sulfoxide at a concentration of 40 mM. The stock solution was stored at –80 °C. For labeling, each mutant was concentrated to 50 μM in buffer A [50 mM 3-(*N*-morpholino) propanesulfonic acid, pH 7.0, 100 mM NaCl, 2.5 mM MgCl<sub>2</sub>, 0.2% *n*-dodecyl-β-D-maltoside] and treated for 20 min at 0 °C with a 8.4-fold molar excess of MTSL over F<sub>0</sub>F<sub>1</sub>. Unbound MTSL was removed by two subsequent passages of the sample through Sephadex G50 fine columns equilibrated with buffer A. The spin-labeled F<sub>0</sub>F<sub>1</sub>-ATP synthase was concentrated for EPR experiments by precipitation in saturated ammonium sulfate (pH 7.5) and dissolving the precipitate in 50 μl buffer A. Ammonium sulfate was removed by two subsequent passages of the sample through Sephadex G50 fine columns equilibrated with buffer A yielding enzyme concentrations in the range from 40 to 110 μM. Samples were stored at –80 °C.

### 2.3. Cross-linking

F<sub>0</sub>F<sub>1</sub>-bT62C and b<sub>34–156</sub>T62C [25] (a truncated b-subunit without amino acids 1 to 33) at a concentration of 10 μM were incubated separately at 23 °C with 50 μM CuCl<sub>2</sub> in buffer A. Reactions were stopped by the addition of 2 mM EDTA after 30 min and 120 min, respectively. 5 μg of protein per lane was used for SDS-PAGE (13%). The gel (shown in Fig. 1c) was stained with Coomassie Blue.

### 2.4. Enzyme activity

F<sub>0</sub>F<sub>1</sub> concentrations were determined by UV absorption using a molecular mass of 550 kDa and a molar extinction coefficient  $\epsilon=340,000 \text{ M}^{-1} \text{ cm}^{-1}$  at 278 nm. For each mutant, ATP synthesis rates were measured at 23 °C by a luciferin/luciferase assay after an acid-base-transition [41]. Samples with an ATP synthesis rate above 20 s<sup>-1</sup> were used for spin labeling.

### 2.5. Control for the specificity of spin labeling

F<sub>0</sub>F<sub>1</sub>-bQ64C was concentrated to 20 μM in buffer A and treated for 90 min at 0 °C with a 1.8-fold molar excess of TMR-M (Molecular Probes, Leiden, The Netherlands) over F<sub>0</sub>F<sub>1</sub>. After removing unreacted dye by passage of the sample through a Sephadex G50 fine column equilibrated with buffer A, the degree of fluorescence labeling was determined and SDS-PAGE was used to visualize the specificity of labeling. The same procedure was performed with spin-labeled b-Q64C.

### 2.6. X-band EPR spectroscopy

9-GHz EPR measurements were carried out using an Elexsys 680 FT/CW spectrometer (Bruker BioSpin GmbH, Rheinstetten, Germany). A dielectric resonator was used. Measurements of free spin-label MTSL and the spin-labeled mutants of F<sub>0</sub>F<sub>1</sub>-ATP synthase were performed in buffer A in liquid solution at room temperature (21 °C). Measurements were performed at 2 mW microwave power using a modulation frequency of 100 kHz with an amplitude of 0.1 mT for samples containing F<sub>0</sub>F<sub>1</sub>-ATP synthase and 0.02 mT for MTSL in buffer A. The total measurement time for spectra of the F<sub>0</sub>F<sub>1</sub>-ATP synthase was 10 min and 20 min for MTSL.

For measurements in frozen solution, 30% glycerol (v/v) was added to the enzyme and the samples were transferred into 4-mm o.d. quartz capillary tubes (Wilma Glass). Measurements were performed at 0.001 mW microwave power using a modulation frequency of 100 kHz with an amplitude of 0.1 mT. Total measurement time was 40 min.

### 2.7. W-band EPR spectroscopy

High frequency (95 GHz) EPR measurements were carried out at 40 K using an Elexsys 680 FT/CW spectrometer (Bruker BioSpin GmbH, Rheinstetten, Germany) with an Oxford 5.8 T split coil magnet as described in [42]. Spectra were measured at 0.05 μW microwave power using a modulation frequency of 100 kHz with an amplitude of 0.5 mT, and a total measurement time of 30 min. Simulations of the frozen solution W-band spectra were performed using the Bruker SimFonia (Bruker BioSpin GmbH, Rheinstetten, Germany) EPR software. The errors of individual parameters were estimated from the minimum

change in the respective parameter resulting in a visible deterioration of the simulation.

### 2.8. DEER experiments

DEER experiments were performed using an Elexsys 680 FT/CW spectrometer (Bruker BioSpin GmbH, Rheinstetten, Germany), modified as described in [43]. Samples for DEER spectroscopy were prepared as described above for the frozen solution X-band EPR experiments, and experiments were performed at 40 K. The four pulse DEER sequence [44]  $p_1-t_1-p_2-t_2-p_3$  with a pump pulse inserted after  $p_2$  was employed. Pulse lengths were 32 ns for  $p_1$ ,  $p_2$  and  $p_3$ , and amplitudes were adjusted to obtain a  $\pi/2$  pulse for  $p_1$  and  $\pi$ -pulses for  $p_2$  and  $p_3$ . The pump-pulse length was 36 ns, and the pump power was adjusted for maximum inversion of the echo. Delay times were  $t_1=200$  ns,  $t_2=2000$  ns and the time  $T$ , at which the pump pulse was inserted after  $p_2$ , was varied. The observer field was set to the low field edge of the spin-label EPR spectrum and the pump frequency adjusted to coincide with the maximum of the nitroxide spin-label EPR signal, resulting in a separation of  $\nu_{\text{pump}}$  and  $\nu_{\text{obs}}$  of 74 MHz. The pulse lengths employed determine the minimum distance accessible by the technique, which is approximately 1.2 nm here.

Simulations of the DEER time traces were performed using the program by Jeschke et al. [38,45,46]. In the case of  $F_0F_1$ -bI40C, the automatic fitting routine converged. For the time traces of the other mutants, the parameters were adjusted manually, and errors were determined by seeking for the minimum change in the respective parameter, resulting in a visible deterioration of the simulation.

## 3. Results

### 3.1. Characterization of the spin-labeled $F_0F_1$ -ATP synthases

The  $F_0F_1$ -ATP synthase of *E. coli* was labeled with spin-label MTSL as described in Materials and methods. To check the specificity of labeling of the b-subunits, we used a differential labeling procedure. First, the Q64C mutant of  $F_0F_1$ -ATP synthase ( $F_0F_1$ -bQ64C) was labeled with the fluorescence label TMR-M; the molecular ratio of bound TMR to  $F_0F_1$ -bQ64C was 1.25. SDS-PAGE shows that mainly the b-subunit was labeled with some minor unspecific labeling of other subunits. In the second experiment,  $F_0F_1$ -bQ64C was first labeled with MTSL and then the spin-labeled sample was additionally labeled with TMR-M. SDS-PAGE reveals that the b-subunit shows only weak fluorescence while other subunits show similar fluorescence intensities as without prior MTSL labeling (see Fig. 1b). These results indicate that MTSL label blocks

further labeling of the b-subunits by TMR, whereas the labeling pattern of the other subunits by TMR is not significantly changed. This implies that MTSL binds specifically to the b-subunits. In this sample, the ratio of bound TMR to  $F_0F_1$  was 0.65. Thus, the degree of labeling of the b-subunit with MTSL was 0.6, which shows that a representative ensemble of the enzyme is labeled. Statistically, the probability that both b-subunits in the holo-enzyme were labeled was 0.09. This low labeling degree was chosen to retain a high selectivity of b-subunit labeling.

### 3.2. Cross-linking experiments with an isolated fragment of the mutant b-subunit ( $b_{34-156}$ T62C) and with $F_0F_1$ -bT62C

Treatment with  $\text{CuCl}_2$  resulted in cross-linking of the isolated b-subunits as shown in Fig. 1c, lanes 5 and 6. The same treatment of  $F_0F_1$ -bT62C does not lead to cross-links between the b-subunits in Fig. 1c (lanes 2 and 3), suggesting a major structural difference between the b-subunit in the solution, for which a dimeric structure had been proposed [22], and in the holo-enzyme.

Spin-labeled  $F_0F_1$ -ATP synthases were incorporated into liposomes to check whether the holo-enzyme is still fully functional. The turnover of the enzyme measured under standard conditions at 23 °C [41] was  $(20 \pm 5) \text{ s}^{-1}$  for ATP synthesis and it decreased to  $(13 \pm 4) \text{ s}^{-1}$  after labeling the same sample with MTSL.

### 3.3. EPR spectroscopy

The following EPR experiments were performed with MTSL labeled  $F_0F_1$  in buffer A: liquid solution X-band EPR to determine mobility, frozen solution X-band and W-band EPR to determine hyperfine and g-tensor components, and, for short distances, spin-spin interactions. Finally, to determine distances above 1.2 nm, double electron-electron resonance (DEER) was used because it is exclusively sensitive to the dipolar interaction between pairs of electron spins.

The liquid solution X-band EPR spectra of all mutants have a similar overall shape. This reveals that there are no large variations in the mobility of the spin label, i.e. that the immediate environment of the spin labels is similar. The spectra resemble those of helix surface sites and have mobility parameters of  $\Delta H^{-1} = 0.25 \text{ G}^{-1}$  (inverse width of central line) and  $\langle H^2 \rangle^{-1} = 3.8 \times 10^{-3} \text{ G}^{-2}$  (inverse second moment) corresponding to helix surface sites or tertiary interaction sites according to the classification of Mchaourab et al. [47,48].

Frozen solution W-band EPR spectra are shown in Fig. 2. The line positions corresponding to the different directions of the nitroxide g-tensor,  $g_x$ ,  $g_y$  and  $g_z$ , are indicated. Spectral simulations of the W-band EPR spectra result in the parameters given in Table 1. The values of  $A_{zz}$  reveal the polarity; those of  $g_x$ , the proteicity of the environment of the

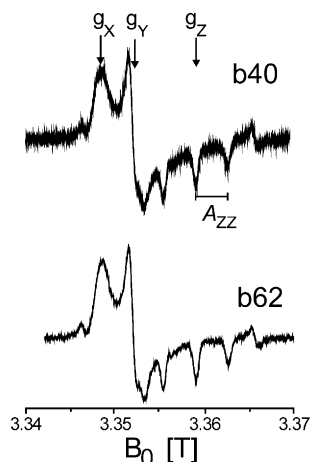


Fig. 2. W-band EPR spectra of spin labels in mutants of  $F_0F_1$ -ATP synthase b-I40C and b-T62C, with spin labels at positions b40 and b62, respectively. Indicated are the resonance fields due to  $g_x$ ,  $g_y$  and  $g_z$  and the hyperfine splitting  $A_{zz}$ .

spin label. The range of  $g_x$  values observed correspond to 13% of the variation seen in  $g_x$  for solvents of different polarity [42], the range of  $A_{zz}$  to 6% of that variation, suggesting that the overall variation in polarity/proteicity between the different sites is small. Differences in  $A_{zz}$  can be neglected, but  $g_x$  for b-T62C and b-Q64C is slightly smaller than for b-I40C, b-H51C and b-D53C, indicating that b-T62C and b-Q64C are in a more protic environment than the remaining mutants, without, however, adopting the values of a solvent-exposed spin label.

The spectra are well described with a single spin, indicating that the dipolar interaction between the spin labels is within the component linewidth ( $\Delta B_i$ , where  $i$  is the direction of the  $g$ -tensor axes  $x$ ,  $y$  and  $z$ ) of the simulation. The magnitude of the unresolved hyperfine components,  $A_{xx}$  and  $A_{yy}$ , and the respective component linewidths,  $\Delta B_x$  and  $\Delta B_y$ , depend on each other. To emphasize differences in

the component linewidth,  $\Delta B_i$ , for all mutants,  $A_{xx}$  and  $A_{yy}$  were kept constant ( $A_{xx}=0.40$  mT and  $A_{yy}=0.45$  mT). Using  $\Delta B_i$  for MTSL as the reference for a single spin label, the difference,  $\Delta$ , in linewidth of the mutant ( $\Delta B_i^{\text{mut}}$ ) relative to MTSL ( $\Delta B_i^{\text{MTSL}}$ ) is calculated as  $\delta_i = \Delta B_i^{\text{mut}} - \Delta B_i^{\text{MTSL}}$ . In all mutants, the largest difference is found along the  $x$  direction  $\delta_x$ , followed by  $\delta_z$ . The values of  $\delta_y$  and  $\delta_z$  are close to their respective experimental errors. For  $\delta_y$ , this is due to the small absolute magnitude of these values; for  $\delta_z$ , this is due to the relatively large experimental error for  $\Delta B_z$ , resulting from baseline drifts, which makes it difficult to get good simulations for the shape of the EPR spectrum in this region. Attributing the increase in linewidth relative to free MTSL to the unresolved dipolar splitting of the two spin labels in the mutants, approximate distances can be obtained from the point-dipolar model (see below).

### 3.4. DEER spectroscopy

DEER time traces characteristic of spin–spin interactions are observed for all mutants. The modulation observed is an unambiguous indication for the intramolecular interaction of two electron spins in the samples. In Fig. 3a, DEER time traces of the mutants are shown. A broad feature at approx.  $0.5 \mu\text{s}$  corresponds to a maximum of the modulation. This feature is most pronounced for the b-I40C, the b-H51C, and the b-D53C mutants. In b-T62C and b-Q64C, this feature is broadened. Additionally, a decay that is almost linear in time is seen in all mutants. This decay, which has different slopes for the different mutants, is due to randomly distributed spins rather than the spin pairs giving rise to the modulation [45]. It is attributed to intermolecular interactions, and the variation observed reflects differences in the total spin concentration, not in the distances themselves. In Fig. 3b, Fourier Transform traces for b-I40C and b-T62C are shown, along with, in Fig. 3c, the corresponding distance distributions (see below).

Table 1  
W-band frozen solution EPR simulation parameters (data normalized to  $g_z=2.00300$ )

	$A_{zz}$ (mT) <sup>a</sup>	$g_x^b$	$g_y$	$\Delta B_x$ (mT) <sup>c</sup>	$\Delta B_y$ (mT) <sup>d</sup>	$\Delta B_z$ (mT) <sup>e</sup>	$\delta_x^f$ (mT)	$\delta_y^g$ (mT)	$\delta_z^h$ (mT)	$r_{\text{min}}$ (nm)
MTSL	3.70	2.00906	2.00687	1.13	0.70	0.65				
b40	3.60	2.00925	2.00686	1.36 <sup>i</sup>	0.76	0.75	0.2 <sup>j</sup>	0.06	0.1	2.0
b51	3.61	2.00925	2.00688	1.43	0.72	0.75	0.3	0.02	0.1	1.8
b53	3.60	2.00924	2.00686	1.34	0.75	0.72	0.2	0.05	0.1	2.1
b62	3.60	2.00915	2.00686	1.20	0.71	0.72	0.1	0.01	0.1	3.0
b64	3.61	2.00917	2.00688	1.27	0.74	0.67	0.1	0.04	0.0	2.4

<sup>a</sup>  $\pm 0.025$  mT.

<sup>b</sup>  $\pm 2 \cdot 10^{-5}$ .

<sup>c</sup> error  $\pm 0.03$  mT.

<sup>d</sup> error  $\pm 0.02$  mT.

<sup>e</sup> error  $\pm 0.04$  mT.

<sup>f</sup>  $\pm 0.06$ .

<sup>g</sup>  $\pm 0.04$ .

<sup>h</sup>  $\pm 0.08$ .

<sup>i</sup> error  $\pm 0.04$  mT.

<sup>j</sup>  $\pm 0.07$ .

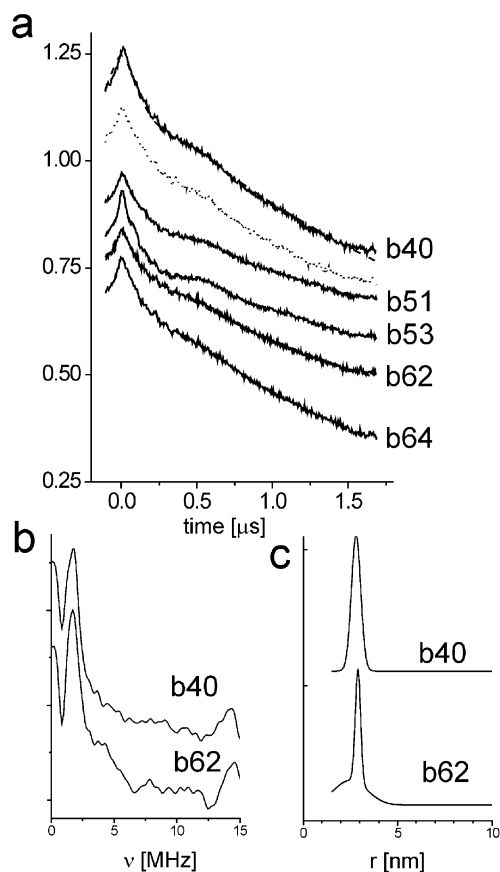


Fig. 3. DEER results on  $F_0F_1$ -ATP synthase. (a) DEER time traces, total measurement times:  $F_0F_1$ -ATP synthase b-I40C (b40) 12.5 h, b40AMPPNP (dotted line) 7 h; b-T51C (b51) 13 h, b-T53C (b53) 12 h, b-T62C (b62) 9 h, b-T64C (b64) 4 h; for further experimental conditions, see text. Dashed lines for b-I40C and b-T62C: simulations using a superposition of distances (see text). (b) Fourier transformation of the DEER time traces of b-I40C and b-T62C. Largest contribution: 1.7 MHz, in b-T62C: broad region of intensity extending to 5.0 MHz. (c) Distance distribution corresponding to the simulations shown in panel a.

### 3.5. Distance information from EPR

The point-dipole model relates the dipolar splitting  $\nu_{\text{dip}}$  observed experimentally with the distances  $r$  between the centers of spin density as [38]:

$$\begin{aligned} \nu_{\text{dip}} &= \frac{52}{r^3} (3\cos^2\theta - 1) [\text{MHz}/\text{nm}^3] \\ &= B_{\text{dip}} (3\cos^2\theta - 1) [\text{MHz}/\text{nm}^3] \end{aligned} \quad (1)$$

where  $\theta$  is the angle between the vector joining the two electron spins and the magnetic field  $B_0$ .

In the W-band cw EPR spectra,  $\nu_{\text{dip}}$  is associated with linewidths  $\delta_i$ . The dipolar broadening of the different components  $i$  in the spectrum depends on the relative orientation of the  $g$ -tensors of the two spin labels. If the  $g$ -tensors are oriented such that, for example, the  $x$ -axes of the  $g$ -tensor are parallel or antiparallel, the largest broadening is expected on the  $x$ -component ( $\delta_x$ ), since in this case  $\theta=0^\circ$  and the splitting  $\delta_x$  is  $2B_{\text{dip}}$ , where  $B_{\text{dip}}$  is the

dipolar splitting for  $\theta=90^\circ$ . In that case, the remaining components  $\delta_y$  and  $\delta_z$  are broadened by  $B_{\text{dip}}$ . Experimentally, positive values for  $\delta_i$  are observed, revealing that the resonances are broadened relative to MTSL. Assuming that positive  $\delta_i$  values are exclusively due to the dipolar interaction of the two electron spins, the distance between the spins can be estimated using the point-dipole model. In the spectra, the largest broadening is found along  $g_x$ , as would be expected, if the  $g_x$ -axes of the spin labels were parallel or antiparallel. The other two components,  $\delta_y$  and  $\delta_z$ , in this case should be broadened by  $\delta_x/2$ . As most of the observed values of  $\delta_y$  are smaller than that, factors other than the dipolar interaction must contribute to  $\delta_x$ . Therefore, the distances,  $r_{\text{min}}$ , calculated from  $\delta_x$  in Table 1 represent a lower limit for the distances of the spin labels in the mutants. For all mutants,  $r_{\text{min}}$  is above 1.8 nm. Therefore, distances smaller than 1.8 nm, in particular distances as small as 1.2 nm, which would result in a broadening of approximately 1.0 mT, can be safely excluded. This is important for the interpretation of the DEER experiments, which are not sensitive to distances smaller than 1.2 nm. The W-band EPR results further explain why X-band EPR frozen-solution spectra did not show substantial differences in linewidth for the mutants. In these spectra, only the lineshape pertaining to  $g_z$  can be determined, which, according to the W-band EPR spectra, shows the smallest variation for the different mutants.

By DEER,  $\nu_{\text{dip}}$  is directly obtained from the Fourier Transform of the time traces, where a maximum is observed at  $\theta=90^\circ$  and orientation effects can be neglected. The Fourier Transformations of the DEER time traces (Fig. 3b) have a peak at 1.7 MHz, corresponding to a distance of approximately 3 nm. For the b-T62C (Fig. 3b) and b-Q64C mutants, also a less intense shoulder is observed, extending from the main peak to 5 MHz, suggesting a contribution of spin pairs with shorter distances down to 2.2 nm. More details were obtained with the program by Jeschke et al. [38,45,46]. The program simulates and fits the DEER time traces with a maximum of two components, each consisting of a Gaussian distribution of distances. For the mutants b-I40C and b-T62C, the resulting simulations of the time traces are shown in Fig. 3a, the distributions of distances in Fig. 3c. The corresponding parameters are given in Table 2. For all mutants, a distance of 2.9 nm is the dominant contribution. The width of the distribution centered at this distance is larger for b-I40C than for the remaining mutants. All mutants except b-I40C have a second component with a broad distribution of distances centered at 2.5 nm, accounting for a minority population of approximately 20% of the spin-label pairs. With respect to this population, for b-H51C and b-D53C the width of the distribution is smaller than for b-T62C and b-Q64C (Table 2). Thus, there must be a larger variability in the local structure of the b-subunits for residues 62 and 64 in the minority population. This could be attributed either to a larger number of conformations of the tether linking the spin label to the protein, or to a larger

Table 2  
Distances from DEER and structural parameters of b-subunit

Mutant	DEER results of component I		DEER results of component II		Amount of II (%)	Structural parameters	
	$r$ (nm) <sup>a</sup>	Width <sup>b</sup> (nm)	$r$ (nm) <sup>c</sup>	Width <sup>d</sup> (nm)		Turn #	Angle (°)
b40	2.94	0.36			0	I	0
b51	2.90	0.20	2.5	1.15	19	III	20
b53	2.95	0.20	2.5	1.15	26	III	220
b62	2.90	0.20	2.5	1.70	22	VI	40
b64	2.90	0.15	2.5	1.70	18	VI	240

<sup>a</sup>  $\pm 0.05$ .

<sup>b</sup> Half-width at half-height.

<sup>c</sup>  $\pm 0.1$ .

<sup>d</sup> Half-width at half-height.

distribution of conformations of the b-subunits with respect to each other. A larger flexibility of the linker can be excluded since it would result in a higher mobility of the spin labels at these positions, which would cause differences in the liquid solution X-band EPR spectra of the respective mutants. This indicates that for a fraction of the enzyme, the part of the b-subunit extending from the tether region to the F<sub>1</sub> binding domain is less well ordered than the section of the b-subunit extending from the F<sub>0</sub> binding domain to the tether region. Given that the corresponding fraction of spin-label pairs is small, we focus on the majority fraction in the following.

The distance of 2.9 nm is consistent with the results of W-band EPR experiments, since it corresponds to a dipolar interaction of 0.06 mT, which should cause  $\delta_i$  parameters of 0.12 or 0.06 mT, depending on the relative orientation of the spin labels. This splitting is comparable to the experimental values,  $\delta_x$ ,  $\delta_y$  and  $\delta_z$  (Table 1). Since, for some of the mutants,  $\delta_x$  is significantly larger than these values, other sources of line-broadening must be present. This makes it impossible to get additional evidence about the heterogeneity from the W-band experiments, or to use these results to determine the relative orientation of the spin labels.

### 3.6. Distance determination with F<sub>0</sub>F<sub>1</sub>-ATP synthases incubated with AMPPNP

Electron microscopy of F<sub>0</sub>F<sub>1</sub>-ATP synthase from *E. coli* combined with three dimensional image reconstruction revealed large conformational changes of the enzyme upon binding of the non-hydrolysable ATP analogue AMPPNP [49]. To investigate whether the binding of AMPPNP changes the distances between the b-subunits, samples of spin-labeled b-I40C, b-H51C and b-Q64C used for DEER experiments before, were thawed, incubated with 5 mM AMPPNP for 30 min and refrozen. As F<sub>0</sub>F<sub>1</sub> concentrations were in the range from 60 to 110  $\mu$ M, AMPPNP binds to all binding sites according to the  $K_d$  values of 0.11  $\mu$ M for the first and 5.5  $\mu$ M for the second and third catalytic binding sites [50]. The DEER traces in the presence of AMPPNP (Fig. 3a) show no significant changes as compared to the traces in its absence.

## 4. Discussion

The F<sub>0</sub>F<sub>1</sub>-ATP synthase from *E. coli* was spin labeled with MTSL at different positions of the b-subunit. Functional assays and SDS-PAGE revealed that labeling was selective, that the spin-labeled enzyme was functional and could be prepared in high concentrations. A relatively low degree of labeling resulted from labeling conditions that were optimized for specific binding, and from differential labeling, a fraction of 0.09 of holo-enzyme with doubly labeled b-subunits was estimated.

The cross-linking experiments give the first indication that the dimeric structure proposed previously for the isolated b-subunits [22] is not retained in the holo-enzyme. The model proposed for this dimer [22] should allow cross-linking by a disulfide bridge at position T62C. As no cross-linked dimers were observed in the holo-enzyme, the interaction of the b-subunits with the F<sub>1</sub>-part and the F<sub>0</sub>-part must be stronger than the interactions between the b-subunits themselves, and the dimeric structure found for isolated b-subunit dimers [22] can be ruled out.

The spin–spin interaction observed in the DEER experiments gives clear evidence that there are two spin labels in the mutants of the b-subunit of F<sub>0</sub>F<sub>1</sub>-ATP synthase, and from the DEER experiments, the actual distances are obtained. As, contrary to the conventional EPR approaches, the DEER technique allows to discriminate between intra- and intermolecular spin–spin interactions, the relatively low yield of doubly labeled protein is not problematic.

The combination of advanced EPR techniques further enabled us to determine the secondary structure element that the mutant is bound to, the polarity of the environment of the spin label and the distance between the spin labels. These results could only be obtained because of the increased spectral resolution of high-field EPR and the sensitivity for long distances of the pulsed EPR technique employed.

### 4.1. Distance information from EPR

The modulation in the DEER experiments (Fig. 3a) shows that both copies of the b-subunit in the mutants can

be spin-labeled. The distance between the centers of spin density, namely the NO-groups of the spin labels, is 2.9 nm. A certain degree of heterogeneity is observed for a minority fraction of the enzyme, from which we conclude that the region of the b-subunits closer to the  $F_1$  binding domain is less well ordered than the section of the b-subunit extending from the  $F_0$  binding domain to the tether region. As the corresponding population of the enzyme only accounts for maximally 20% of the population, we focus on the majority of contribution with the distance of 2.9 nm. To obtain structural information on the b-subunits, the distance between the NO-group and the  $C_\beta$  atoms to which the spin labels are linked is needed. Information on the length and the conformation of the linker in the MTSL spin label has been obtained from X-ray crystallography on a spin-labeled protein [51]. The length of the linker with the spin label in an extended conformation is around 0.56 nm. Therefore, the distance of 2.9 nm observed in the DEER experiment for the spin-label pairs implies that the  $C_\beta$  atoms to which the spin-labels are linked are minimally 1.8 nm apart. This is fully consistent with the failure to obtain cross-linked cystine-dimers of the b-subunits in the holo-enzyme. An upper limit for the distances can be estimated from the results of [17], where a bifunctional dye with a length of about 5 nm was able to cross-link the b-subunits. This excludes distances above 5 nm.

#### 4.2. Spin-label mobility and environment

The magnetic resonance parameters obtained by EPR give information on the location and the environment of the spin label. With respect to these parameters, the spin–spin interaction is a small perturbation, therefore, the parameters can be discussed in terms of the combined properties of the spin labels at both b-subunits.

From the similarity of the liquid solution X-band EPR spectra, it is concluded that the mobility of the spin label is comparable for all mutants. The line shape can be classified as that of a spin label at a somewhat immobilized helix site [51,52], as found for example for sites in the interaction region of two helices in T4 lysozyme [47]. The hyperfine and g-tensor parameters, specifically  $A_{zz}$  and  $g_x$  from W-band EPR (see Table 1), reveal that the polarity and proteicity of the environment at all positions of the spin label are similar. The parameters suggest a location close to, but not fully exposed to, the buffer/detergent environment of the protein. Small differences of  $A_{zz}$  and  $g_x$  between the mutants show that the spin labels at positions b-T62C and b-Q64C are in a more protic, i.e. more buffer like, environment than those at the other positions.

#### 4.3. Model for the structure of the b-subunits in the holo-enzyme

The distance of 1.9 nm between  $C_\beta$  atoms excludes an in-register coiled-coil arrangement of the helices. In the

following, we discuss the implications of this finding with respect to possible relative orientations of the helices. Specifically, we will suggest two models, which are in accordance with the measured distances.

The interpretation is based on an  $\alpha$ -helical structure of the b-subunit in this region [22]. In an  $\alpha$ -helix, the relative orientation of the amino acids is determined by the fact that a full helical turn requires 3.6 residues. Choosing b-I40C arbitrarily as the reference at  $0^\circ$ , the angles of the other mutated amino acids relative to b-I40C are obtained (Table 2). As can be seen in Fig. 4a, b-I40C, b-H51C and b-T62C are at the same side of the helix, albeit at different heights, whereas residues b-D53C and b-Q64C are approximately  $180^\circ$  away from the former group, i.e. at the opposite side of the helix. In both models, this relative orientation of the mutated amino acids within one helix is kept constant. The rotational orientation of the two b-subunits is the same for both models and as shown in Fig. 4b and c. The helices are shifted relative to each other until the model describes correctly the experimentally observed distances.

The first scenario (model (1)) assumes that the helices are in-register, i.e. every pair of amino acids is at the same height. Since the spin-labeled residues at the two helices point in the same direction, it stands to reason that the attached nitroxide labels also point in the same direction. For this reason, the length of the linker of the spin labels can be neglected and the distance measured corresponds to the distance between the  $C_\beta$  atoms to which the labels are bound. Assuming a diameter of 1.0 nm for the helix leads to a separation of the helices by a distance of 1.9 nm. This would imply that there are no significant interactions between the two b-subunits (see Fig. 4b) in the region between residues b-40 and b-64.

In model (2), we assume a direct contact between both helices. Because the diameter of one helix is about 1 nm, this requires that one helix is shifted parallel to the helix axis about 2.7 nm to obtain a distance of 2.9 nm for all mutated amino acids. The shift of 2.7 nm implies a shift of about 20 amino acids or 5 to 6 helical turns (Fig. 4c). In both models, the distances of 2.9 nm between the  $C_\beta$  atoms of the mutated residues are indicated by lines (Fig. 4b and c).

We stress that the two models represent extreme conformations. It would be equally compatible with the data if the two helices were further apart than in model 2 and were shifted less along the long axis of the helix. Our results clearly exclude the close-contact coiled-coil arrangements of the b-subunits that had been proposed previously based on the results of measurements of isolated b-subunits in solution. The structural information about these dimers is summarized in the Introduction. It is well established that soluble b-monomers (e.g. b<sub>54–143</sub>) form such dimers in solution and that their properties, such as dissociation constants, depend on the properties of the medium (pH,  $Mg^{2+}$  concentration, etc.), [26], suggesting

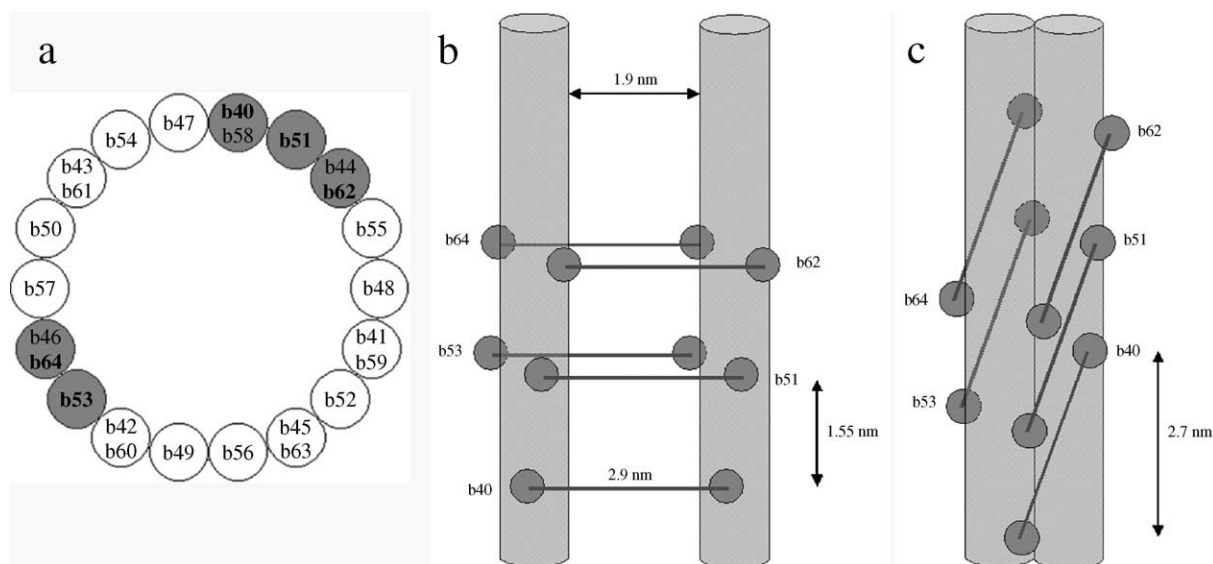


Fig. 4. Models of arrangement of the two b-subunits. (a) Helical wheel projection of the b-subunit assuming a right-handed  $\alpha$ -helix (residues 40 to 64) viewed from  $F_0$ . Spin-labeled residues are shown as balls. The angle between residue 40 and the other spin-labeled residues is given in Table 2. (b) Side view of model (1). Balls indicate the spin-labeled residues; lines indicate the distance of 2.9 nm between spin-labeled residues. The two b-subunits are in-register; residues and spin labels point in the same direction. The two helices have no interaction and are separated by about 1.9 nm. (c) Side view of model (2). The two helices have direct contact. One helix has been shifted to yield a distance of 2.9 nm between the two spin labels. This shift is about 2.7 nm, i.e. 20 amino acids or 5 to 6 helical turns.

that also the structures depend on the mode of preparation. The model of the b-dimer from position 62 to 122 calculated from two monomers in solution [22] proposes a close contact between the two helices with an in-register arrangement of the helices. As also the rotational orientation of the helices differs from the model shown in Fig. 4b, it results in much shorter distances for the mutated residues b-T62C and b-Q64C than observed in the DEER experiments. That these structures do not reflect the arrangement of the b-subunits in the holo-enzyme is most likely due to the anchoring of the b-subunits in the holo-enzyme. It seems that anchoring of the N-termini of the b-subunits in the transmembrane  $F_0$ -part and of the C-terminal region in the  $F_1$ -part affects the relative arrangement of the two b-subunits more strongly than do interactions between the b-subunits, which determine the solution structures of isolated b-subunits. Consequently, it is not surprising that we find significant deviations from these models, such as a significantly larger separation of the two b-subunits in the holo-enzyme.

The arrangement of the two b-subunits seems not to change within experimental error when the substrate analogue AMPPNP is bound. Although the distribution of distances of b-T62C and b-Q64C for the majority of spin-label pairs is relatively large, a change in conformation should be detectable within a limit of 0.05 nm as revealed by simulation of the DEER time traces. With respect to the minority contribution with the wide distance distribution, the error margins are significantly larger. However, differences in the width of the distribution of 1.15 nm (b-H51C and b-D53C) and 1.70 nm (b-T62C and b-Q64C) can be clearly distinguished, suggesting that potential distance changes are well below 0.55 nm, also for that fraction of

the protein. The required storage of mechanical energy during the working cycle of the enzyme, therefore, does not seem to involve the relative motion of the two helices with respect to each other.

In summary, we find that the EPR experiments confirm the more protic environment of the b-subunit close to the head region of the enzyme. The failure to obtain cross-linked b-subunit dimers in the holo-enzyme and the relatively large distance observed by DEER exclude a coiled-coil arrangement of the b-subunits and lead us to the proposal of a new model for the structure of the enzyme with respect to the b-subunits. No evidence of relative motion of the b-subunits due to the binding of the ATP-analogue was found, suggesting that the storage of mechanical energy during enzymatic function does not involve such a motion of the b-subunits.

## Acknowledgements

We thank R. Reuter for mutagenesis work, W. Wangler for his help to prepare the enzyme, and S.D. Dunn for the gift of the isolated truncated b-monomer  $b_{34-156}$ T62C. We gratefully acknowledge the participation of M. Finiguerra in the EPR experiments and thank G. Kothe for his helpful comments. The invaluable continuous support from E.J.J. Groenen and J. Schmidt is gratefully acknowledged. This work was performed under the auspices of the BIOMAC research school of Leiden University and was financially supported by the Studienstiftung des deutschen Volkes (Bonn, Germany), the Marie-Curie Training Site at Leiden University by the European Union, and the Dutch Science Organization NWO-CW.

## References

- [1] P. Mitchell, Coupling of phosphorylation to electron and hydrogen transfer by a chemi-osmotic type of mechanism, *Nature* 191 (1961) 144–152.
- [2] R.H. Fillingame, O.Y. Dmitriev, Structural model of the transmembrane  $F_0$  rotary sector of  $H^+$ -transporting ATP synthase derived by solution NMR and intersubunit cross-linking in situ, *Biochim. Biophys. Acta* 1565 (2002) 232–245.
- [3] H. Seelert, A. Poetsch, N.A. Dencher, A. Engel, H. Stahlberg, D.J. Müller, Structural biology: Proton-powered turbine of a plant motor, *Nature* 405 (2000) 418–419.
- [4] P.D. Boyer, ATP synthase—past and future, *Biochim. Biophys. Acta* 1365 (1998) 3–9.
- [5] J.P. Abrahams, A.G.W. Leslie, R. Lutter, J.E. Walker, Structure at 2.8 Å resolution of  $F_1$ -ATPase from bovine heart-mitochondria, *Nature* 370 (1994) 621–628.
- [6] T.M. Duncan, V.V. Bulygin, Y. Zhou, M.L. Hutcheon, R.L. Cross, Rotation of subunits during catalysis by *Escherichia coli*  $F_1$ -ATPase, *Proc. Natl. Acad. Sci. U. S. A.* 92 (1995) 10964–10968.
- [7] D. Sabbert, S. Engelbrecht, W. Junge, Intersubunit rotation in active  $F_1$ -ATPase, *Nature* 381 (1996) 623–625.
- [8] H. Noji, R. Yasuda, M. Yoshida, K. Kinosita, Direct observation of the rotation of  $F_1$ -ATPase, *Nature* 386 (1997) 299–302.
- [9] S. Engelbrecht, W. Junge, ATP synthase: a tentative structural model, *FEBS Lett.* 414 (1997) 485–491.
- [10] M. Yoshida, E. Muneyuki, T. Hisabori, ATP synthase—A marvelous rotary engine of the cell, *Nat. Rev., Mol. Cell Biol.* 2 (2001) 669–677.
- [11] R.A. Capaldi, R. Aggeler, Mechanism of the  $F_1F_0$ -type ATP synthase, a biological rotary motor, *Trends Biochem. Sci.* 27 (2002) 154–160.
- [12] J. Weber, A.E. Senior, ATP synthesis driven by proton transport in  $F_1F_0$ -ATP synthase, *FEBS Lett.* 545 (2003) 61–70.
- [13] T. Elston, H.Y. Wang, G. Oster, Energy transduction in ATP synthase, *Nature* 391 (1998) 510–513.
- [14] D. Sabbert, W. Junge, Stepped versus continuous rotatory motors at the molecular scale, *Proc. Natl. Acad. Sci. U. S. A.* 94 (1997) 2312–2317.
- [15] O. Pänke, B. Rumberg, Kinetic modeling of rotary  $CF_0F_1$ -ATP synthase: storage of elastic energy during energy transduction, *Biochim. Biophys. Acta* 1412 (1999) 118–128.
- [16] M. Börsch, M. Diez, B. Zimmermann, R. Reuter, P. Gräber, Stepwise rotation of the gamma-subunit of  $EF_0F_1$ -ATP synthase observed by intramolecular single-molecule fluorescence resonance energy transfer, *FEBS Lett.* 527 (2002) 147–152.
- [17] M. Diez, B. Zimmermann, M. Börsch, M. König, E. Schweinberger, S. Steigmiller, R. Reuter, S. Felekyan, V. Kudryavtsev, C.A.M. Seidel, P. Gräber, Proton-powered subunit rotation in single membrane-bound  $F_0F_1$ -ATP synthase, *Nat. Struct. Mol. Biol.* 11 (2004) 135–141.
- [18] B. Böttcher, L. Schwarz, P. Gräber, Direct indication for the existence of a double stalk in  $CF_0F_1$ , *J. Mol. Biol.* 281 (1998) 757–762.
- [19] S. Wilkens, R.A. Capaldi, Electron microscopic evidence of two stalks linking the  $F_1$  and  $F_0$  parts of the *Escherichia coli* ATP synthase, *Biochim. Biophys. Acta* 1365 (1998) 93–97.
- [20] S. Karrasch, J.E. Walker, Novel features in the structure of bovine ATP synthase, *J. Mol. Biol.* 290 (1999) 379–384.
- [21] O. Dmitriev, P.C. Jones, W.P. Jiang, R.H. Fillingame, Structure of the membrane domain of subunit b of the *Escherichia coli*  $F_0F_1$  ATP synthase, *J. Biol. Chem.* 274 (1999) 15598–15604.
- [22] P.A. Del Rizzo, Y. Bi, S.D. Dunn, B.H. Shilton, The “second stalk” of *Escherichia coli* ATP synthase: structure of the isolated dimerization domain, *Biochemistry* 41 (2002) 6875–6884.
- [23] S.D. Dunn, D.T. McLachlin, M. Revington, The second stalk of *Escherichia coli* ATP synthase, *Biochim. Biophys. Acta* 1458 (2000) 356–363.
- [24] A.J.W. Rodgers, R.A. Capaldi, The second stalk composed of the b- and delta-subunits connects  $F_0$  to  $F_1$  via an alpha-subunit in the *Escherichia coli* ATP synthase, *J. Biol. Chem.* 273 (1998) 29406–29410.
- [25] M. Diez, M. Börsch, B. Zimmermann, P. Turina, S.D. Dunn, P. Gräber, Binding of the b-subunit in the ATP Synthase from *Escherichia coli*, *Biochemistry* 43 (2004) 1054–1064.
- [26] J. Weber, S. Wilke-Mounts, S. Nadanaciva, A.E. Senior, Quantitative determination of direct binding of b subunit to  $F_1$  in *Escherichia coli*  $F_1F_0$ -ATP synthase, *J. Biol. Chem.* 279 (2004) 11253–11258.
- [27] M. Futai, T. Noumi, M. Maeda, ATP synthase ( $H^+$ -ATPase)—Results by combined biochemical and molecular biological approaches, *Ann. Rev. Biochem.* 58 (1989) 111–136.
- [28] S.D. Dunn, The polar domain of the b-subunit of *Escherichia coli*  $F_1F_0$ -ATPase forms an elongated dimer that interacts with the  $F_1$  sector, *J. Biol. Chem.* 267 (1992) 7630–7636.
- [29] K.A. Mc Cormick, G. Deckers-Hebestreit, K. Altendorf, B.D. Cain, Characterization of mutations in the b-subunit of  $F_1F_0$  ATP synthase in *Escherichia coli*, *J. Biol. Chem.* 268 (1993) 24683–24691.
- [30] K. Altendorf, W.D. Stalz, J.C. Greie, G. Deckers-Hebestreit, Structure and function of the  $F_0$  complex of the ATP synthase from *Escherichia coli*, *J. Exp. Biol.* 203 (2000) 19–28.
- [31] J.C. Greie, G. Deckers-Hebestreit, K. Altendorf, Secondary structure composition of reconstituted subunit b of the *Escherichia coli* ATP synthase, *Eur. J. Biochem.* 267 (2000) 3040–3048.
- [32] M. Revington, D.T. McLachlin, G.S. Shaw, S.D. Dunn, The dimerization domain of the b subunit of the *Escherichia coli*  $F_1F_0$ -ATPase, *J. Biol. Chem.* 274 (1999) 31094–31101.
- [33] T.B. Grabar, B.D. Cain, Integration of b subunits of unequal lengths into  $F_1F_0$ -ATP synthase, *J. Biol. Chem.* 278 (2003) 34751–34756.
- [34] D.T. McLachlin, A.M. Coveny, S.M. Clark, S.D. Dunn, Site-directed cross-linking of b to the alpha, beta, and a subunits of the *Escherichia coli* ATP synthase, *J. Biol. Chem.* 275 (2000) 17571–17577.
- [35] M.V. Kersten, S.D. Dunn, J.G. Wise, P.D. Vogel, Site-directed spin-labeling of the catalytic sites yields insight into structural changes within the  $F_0F_1$ -ATP synthase of *Escherichia coli*, *Biochemistry* 39 (2000) 3856–3860.
- [36] P.D. Vogel, Insights into ATP synthase structure and function using affinity and site-specific spin labeling, *J. Bioenerg. Biomembr.* 32 (2000) 413–421.
- [37] T. Hornung, D.T. McLachlin, S.D. Dunn, E.J. Hustedt, J.G. Wise, P.D. Vogel, The second stalk of  $F_0F_1$ -ATP-synthase, *Biophys. J.* 86 (2004) 337A.
- [38] G. Jeschke, Distance measurements in the nanometer range by pulse EPR, *Chemphyschem.* 3 (2002) 927–932.
- [39] M. Persson, J.R. Harbridge, P. Hammarstrom, R. Mitri, L.G. Martensson, U. Carlsson, G.R. Eaton, S.S. Eaton, Comparison of electron paramagnetic resonance methods to determine distances between spin labels on human carbonic anhydrase II, *Biophys. J.* 80 (2001) 2886–2897.
- [40] P.P. Borbat, H.S. Mchaourab, J.H. Freed, Protein structure determination using long-distance constraints from double-quantum coherence ESR: study of T4 lysozyme, *J. Am. Chem. Soc.* 124 (2002) 5304–5314.
- [41] S. Fischer, P. Gräber, Comparison of  $\Delta pH$ - and  $\Delta\phi$ -driven ATP synthesis catalyzed by the  $H^+$ -ATPases from *Escherichia coli* or chloroplasts reconstituted into liposomes, *FEBS Lett.* 457 (1999) 327–332.
- [42] R. Owenius, M. Engstrom, M. Lindgren, M. Huber, Influence of solvent polarity and hydrogen bonding on the EPR parameters of a nitroxide spin label studied by 9-GHz and 95-GHz EPR spectroscopy and DFT calculations, *J. Phys. Chem., A* 105 (2001) 10967–10977.
- [43] I.M.C. van Amsterdam, M. Ubbink, G.W. Canters, M. Huber, Measurement of a Cu–Cu distance of 26 Å by a pulsed EPR method, *Angew. Chem., Int. Ed. Engl.* 42 (2003) 62–64.
- [44] M. Pannier, S. Veit, A. Godt, G. Jeschke, H.W. Spiess, Dead-time free measurement of dipole–dipole interactions between electron spins, *J. Magn. Res.* 142 (2000) 331–340.

- [45] G. Jeschke, A. Koch, U. Jonas, A. Godt, Direct conversion of EPR dipolar time evolution data to distance distributions, *J. Magn. Res.* 155 (2002) 72–82.
- [46] G. Jeschke, Determination of the nanostructure of polymer materials by electron paramagnetic resonance spectroscopy, *Macromol. Rapid Commun.* 23 (2002) 227–246.
- [47] H.S. Mchaourab, M.A. Lietzow, K. Hideg, W.L. Hubbell, Motion of spin-labeled side chains in T4 lysozyme, correlation with protein structure and dynamics, *Biochemistry* 35 (1996) 7692–7704.
- [48] J.M. Isas, R. Langen, H.T. Haigler, W.L. Hubbell, Structure and dynamics of a helical hairpin and loop region in annexin 12: a site-directed spin labeling study, *Biochemistry* 41 (2002) 1464–1473.
- [49] B. Böttcher, J. Bertsche, R. Reuter, P. Gräber, Direct visualisation of conformational changes in  $EF_0F_1$  by electron microscopy, *J. Mol. Biol.* 296 (2000) 449–457.
- [50] J. Weber, A.E. Senior, Catalytic mechanism of  $F_1$ -ATPase, *Biochim. Biophys. Acta* 1319 (1997) 19–58.
- [51] R. Langen, K.J. Oh, D. Cascio, W.L. Hubbell, Crystal structures of spin labeled T4 lysozyme mutants: implications for the interpretation of EPR spectra in terms of structure, *Biochemistry* 39 (2000) 8396–8405.
- [52] L. Columbus, T. Kalai, J. Jeko, K. Hideg, W.L. Hubbell, Molecular motion of spin labeled side chains in alpha-helices: analysis by variation of side chain structure, *Biochemistry* 40 (2001) 3828–3846.